

DYNAMIC RESPONSE OF THE MICRO-PERFORATED CRAB BEAM USED IN MEMS VIBRATORY GYROSCOPE DEVICE

Vu Van The[✉]

Le Quy Don Technical University, Hanoi, Vietnam

E-mail: vuvanthe@lqdtu.edu.vn

Received: 23 November 2023 / Revised: 04 January 2024 / Accepted: 25 January 2024

Published online: 22 February 2024

Abstract. This paper presents a study on the dynamic response of the micro-beams with the crab shape and cut-out holes on the whole operating faces of the beam to create the micro-perforated beam by using FEM simulation software. The obtained results show that the size and shape form of the cut-out holes affect the mechanical responses of the beam on which the holes distribute. The equivalent stiffness of perforated micro-beams decreases significantly with the increasing size of the holes on the beam operating face. And thence the major frequencies of the MEMS vibratory gyroscope system that consist of these micro-beams also decrease. The results of the study are basic for being used for optimizing the structure in subsequent research.

Keywords: cut-out hole, mechanical response, micro crab beam, MEMS.

1. INTRODUCTION

Beams play an essential role in forming the motion of the mechanical vibration systems. They are considered the springs in mechanical vibration systems thanks to the elasticity of the material of the beams. Their displacement under excited loads causes the desired vibration modal in the mechanical system. In micro-electro-mechanical systems (MEMS), the mechanical designs play essential roles in performing the main function of the microsensor or microactuator. The micro-beams in MEMS can be formed as the single model [1], folder model [2,3], Crab-shaped model [3], multi-folder model [1–4], T-shaped model [4], Z-shaped and V-shaped model [5]. The mechanical response of these beams was studied with full fill mode with the constant cross-section and using the assumptions in the analysis processing to consider the elastic behavior of material to be linear and ignore the large deformation of structures.

The perforations cutout along the beams are considered very common in MEMS fabrication. They are created in the sacrificial layer etching process. They cause the reduction in the mass of the beam which in turn decreases the residual stress of the beam and also contributes to reducing pull-in voltage on these beams [6]. The holes perforated on the body of the beam and the body of the resonant have been shown as a solution to reduce the effective mass of the beam as well as the effect of squeeze film damping on them. These two are the major factors affecting the switching time of MEMS switches [7]. Decreasing the effective mass and increasing the active area are the basis for increasing the sensitivity of the MEMS resonators [8]. The perforated holes were shown that they have very little effect on pull-in voltage even though they reduce both the equivalent stiffness and the effective Young's modulus of the meander flexure MEMS switch [9].

The single beam is considered and calculated by using Euler Bernoulli or Timoshenko beam theory based on assumptions that the total induced stress throughout the cross section is the same for both fully filled and the corresponding perforated one and the stress distribution throughout the filled segment in the perforated nanobeam is assumed to be linear and continuous [10–12]. Some different types of beams were also considered based on this approach to define their dynamic characteristics in the vibration problem. However, the dynamic response of the complex shape beam with perforated holes has not yet been researched due to complexity in modeling. Research optimizing mechanical structure to reduce self-weight, thereby reducing energy consumption and ensuring accuracy for MEMS components is an essential requirement. Therefore, it is necessary to study the dynamic responses of perforated beams to determine the vibration characteristics of the mechanical system in mems devices.

In this paper, a microbeam with the “Crab” shape in structure and square or circle-shaped perforated holes will be presented. Therefore, a microelectromechanical vibratory gyroscope model with this crab beam will be considered to determine the mechanical characteristics of the whole system with perforated holes. The content focuses on dynamic analysis to determine the equivalent stiffness and modal analysis to find out the resonant frequency in desired motions.

2. PERFORATED MICRO CRAB-SHAPE BEAM MODEL

The configuration of the Crab-shaped beam is presented in Fig. 1. The cutout holes are distributed uniformly on the operating face parallel to the motion plane. The beam with full-fill bodies is commonly used in designing MEMS structures. However, perforations in the body of the beam and its mechanical responses still need to be considered to obtain the properties of the whole mechanism.

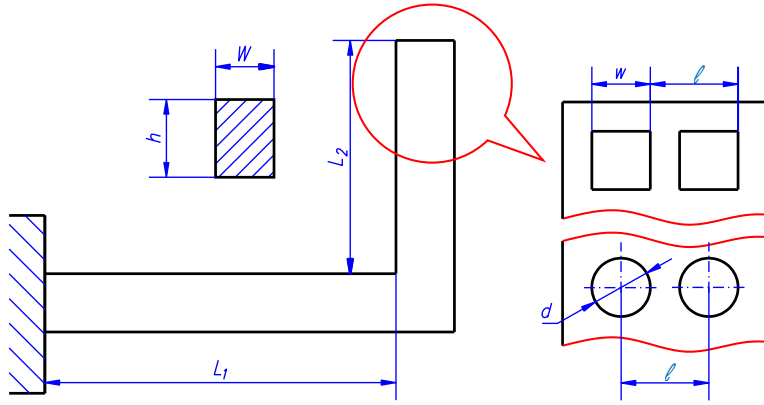


Fig. 1. The configuration of the micro crab beam with cutout holes

Each crab beam is formed from 2 single beam segments considered as the Timoshenko or Euler Bernoulli beams. The length and width of the beams are L and W , respectively. The thickness of beams is h , so the cross-section in a rigid body is $W \times h$. The square holes (edge w) or circle holes are distributed on the working surface plane of the beams at a meshed grid l .

To consider the influence level of the cutout holes in the whole structure, the fill factor is mentioned as the ratio of hole size (w or d) to meshed grid l [8, 11].

$$\alpha = 1 - w/l \quad \text{or} \quad \alpha = 1 - d/l, \quad (1)$$

Thereby, $0 \leq \alpha \leq 1$, $\alpha = 0$ corresponds to the artificial case (cutout whole beam, $d = l$ or $w = l$), and $\alpha = 1$ is the fully filled solid beam (no hole cutout, $w = d = 0$). The smaller the value of the fill factor, the larger the hole size. In this paper, the value $\alpha = 0$ will not be considered to ensure continuity in the models built in simulation calculations.

The material used regularly for these beams is Silicon in SOI wafers with material characteristics: density $\rho = 2330 \text{ kg/m}^3$; Poisson's ratio $\nu = 0.28$; Young's modulus $E = 169 \times 10^9 \text{ Pa}$; Bulk modulus $1.2803 \times 10^{11} \text{ Pa}$; and orientation 1-0-0.

3. MECHANICAL RESPONSE OF PERFORATED MICROSTRUCTURES

3.1. Basic Timoshenko and Euler–Bernoulli perforated beam theory

The basic Timoshenko or Euler–Bernoulli beam theory when taking into account the perforated holes with the square shape was carried out by using an equivalent geometrical model [10] and considering the coupled effect of microstructure and surface stress under different loading and boundary conditions (simply supported, clamped-clamped,

simply-clamped, clamped-guided, or clamped-free, ...) [8]. The Timoshenko beam theory takes into account the shear deformation and axial deformation of the beam, as well as the bending deformation. The cross-section of the beam is allowed to deform as the beam bends, and the beam is modeled as a series of curved line segments. This allows for more accurate modeling of the shear deformation and axial deformation of the beam, which can be important for short, thick beams or beams subjected to high shear loads. As a result, the shape of a Timoshenko beam under bending deformation is more complex than that of an Euler–Bernoulli beam, with a varying curvature along the length of the beam.

To find out the resonant frequencies of the single beams considered Timoshenko beams [10, 11], their dynamic equations are written as follows [12]:

$$EI \frac{\partial^4 u}{\partial x^4} + \rho A \frac{\partial^2 u}{\partial t^2} - \left(\rho I + \frac{EI\rho A}{GA} \right) \frac{\partial^4 u}{\partial x^2 \partial t^2} + \frac{\rho I \rho A}{GA} \frac{\partial^4 u}{\partial x^4} = p(x, t) + \frac{\rho I}{GA} \frac{\partial^2 p(x, t)}{\partial t^2}, \quad (2)$$

where $u = u(x, t)$ is the displacement of the beam; $p(x, t)$ is the distributed load applied to the surface of the beam; and EI , ρA , GA , and ρI are the bending stiffness, linear density, shear stiffness, and rotational moment of the oscillator, respectively.

Considering $u(x, t) = U(x) \cos \omega t$ and neglecting the moment of inertia related to the rotation of the beam element, the shear beam equation can be given as:

$$EI \frac{d^4 U}{dx^4} - \rho A \omega^2 U + \frac{EI\rho A}{GA} \omega^2 \frac{d^2 U}{dx^2} = 0. \quad (3)$$

In the boundary condition case of a clamped-clamped single beam, the natural frequency of the structure is determined by the expression [10]:

$$f_n = \frac{1}{2\pi} \sqrt{\frac{EI_{eq} Z^4}{\rho A_{eq} L^4}}, \quad (4)$$

where EI_{eq} and ρA_{eq} are the bending stiffness and the mass per unit length of the perforated beam, L is the length of the beam, and Z is a function representing the n^{th} root of the equation as a function of γ considered as a geometry-dependent variable:

$$\gamma = \frac{EI_{eq}}{AG_{eq} L^2}, \quad (5)$$

AG_{eq} is the shear stiffness of the perforated beam.

$$EI_{eq} = EI \frac{(N+1)\alpha(N^2+2N+\alpha^2)}{(1-\alpha^2+\alpha^3)N^3+3\alpha N^2+(3+2\alpha-3\alpha^2+\alpha^3)\alpha^2 N+\alpha^3}, \quad (6)$$

$$AG_{eq} = A \frac{N+1}{N} \frac{E}{2} \alpha^3.$$

For perforated beams, γ can be expressed as a function of the number of holes along the section N and fill factor α :

$$\gamma = \frac{1}{6} \left(\frac{W}{L} \right)^2 \gamma_F(N, \alpha) \ll 1, \quad (7)$$

where $\gamma_F(N, \alpha)$ is an appropriate rational function of its arguments:

$$\gamma_F = \frac{N(N^2 + 2N + \alpha^2)}{\alpha^2((\alpha^3 - \alpha^2 + 1)N^3 + 3\alpha N^2 + \alpha^2(\alpha^3 - 3\alpha^2 + 2\alpha + 3)N + \alpha^3)}. \quad (8)$$

This frequency can be determined by the expression used to compare in [13] as follows:

$$f_n = \frac{n\pi}{2L} \sqrt{\left(\frac{EI}{\rho I} \right) \left(B_n - \sqrt{B_n^2 - \frac{\kappa GA}{\pi^4 EI} \frac{\rho I}{\rho A}} \right)}, \quad (9)$$

where $B_n = \frac{1}{2\pi^2} + \frac{\kappa GA}{2\pi^4 EI} \left(\frac{\rho I}{\rho A} \pi^2 + \frac{L^2}{n^2} \right)$.

In the case of the Euler–Bernoulli beam with the assumption that plane sections perpendicular to the axis of the beam before deformation remain plane, and rotate such that they remain perpendicular to the (deformed) axis after deformation, the natural frequencies can be defined by the following expression [14]:

$$\omega_n^2 = \frac{\left(\frac{n\pi}{L} \right)^4 \left(\frac{K_b}{I_0} \right)}{1 + \left(\frac{I_1}{I_0} \right) \left(\frac{n\pi}{L} \right)^2}, \quad (10)$$

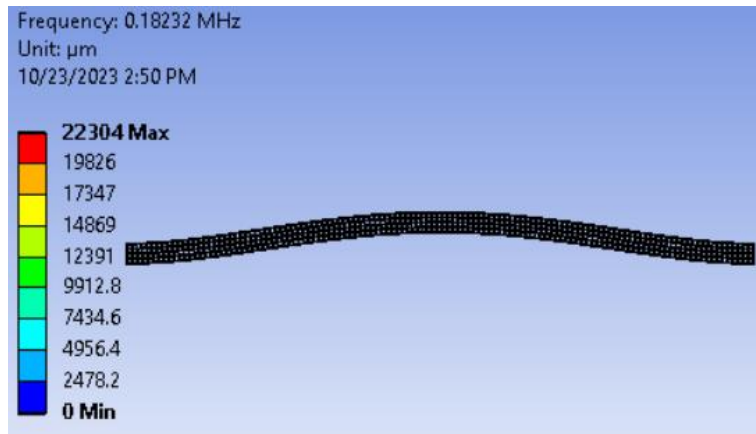
where K_b is the equivalent bending stiffness of the beam; $I_1 = \rho I_{eq}$ and $I_0 = \rho I_{eq}$ refer to the equivalent rotary inertia and the equivalent mass per unit length.

To compare the frequency of the perforated single beam with taking into account the hole in the body of the beam, we consider the referred clamped-clamped beam with 1401.1 μm length, 46.9 μm width, and 60 μm thick [10]. In [10], this structure was modeled as 2D structures (mesh with the element PLANE182) under a plane stress hypothesis corresponded to the case of beams of negligible thickness. In addition, in this study, the body beam is perforated with 4 lines of square holes. The total is 4×116 holes. The beam material chosen is the same with [10] by [1-1-0] single crystal silicon with Young's modulus $E = 169$ GPa, Poison's ratio $\nu = 0.064$, and shear modulus $G = 79.6$ GPa. The 3D structure of this beam and determining its natural frequency is carried out by using ANSYS software with 3D mesh element Hexa20 (6 faces, 20 nodes). The meshing technique used is evenly dividing the surface. The results with fill factor $\alpha = 0.282$ are listed in Table 1. It can be seen with a good agreement between the simulated calculation in this

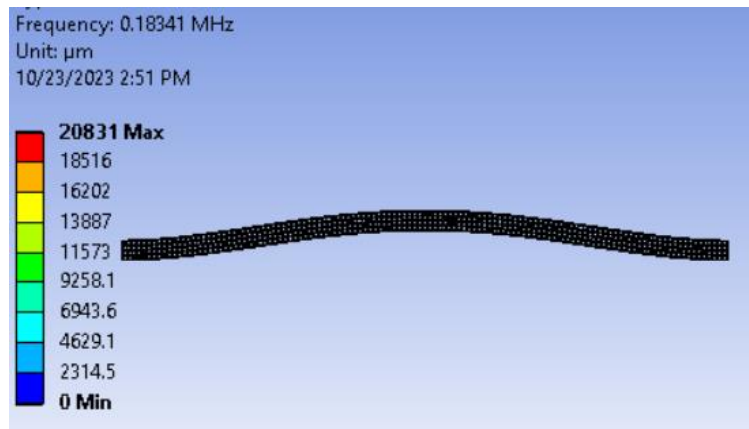
present study and the experimental measurement in [10] with 0.426% error in Table 1. The 3D capture for the displacement and the frequency for the first vibration mode are shown in Fig. 2.

Table 1. The natural frequency of the perforated beam (kHz)

| α | [10] | | | Present study | Error % |
|----------|----------|-------|-------|---------------|---------|
| | Measured | Model | FEM | | |
| 0.282 | 183.1 | 182.3 | 182.2 | 182.32 | 0.426 |



(a) Single beam with square holes



(b) Single beam with circle holes

Fig. 2. The first frequency of the single perforated beam in ANSYS

The change of the first frequency value of the single beam versus the fill factor with $\alpha = 0.05 \div 1$ is shown in Fig. 3.

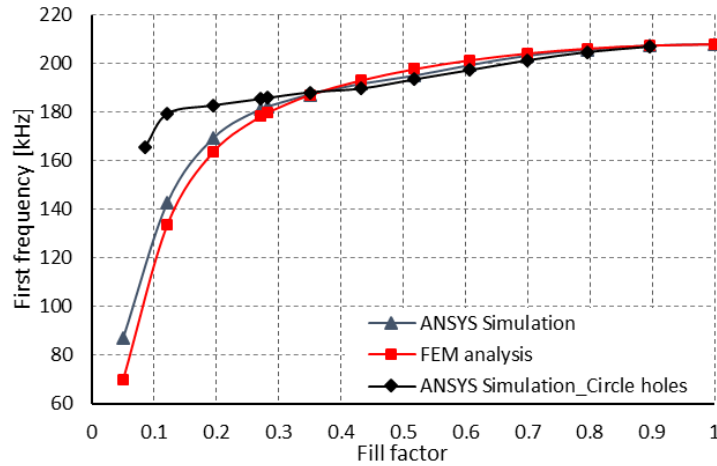


Fig. 3. The first frequency of the referred single beam with fill factor

Based on the finite element analysis method and simulation using ANSYS software, the first two frequencies of single beams with different boundary conditions will be also presented. The outer dimension of the beam $L \times W \times h$ is $1200 \times 120 \times 60$ in micrometer, accordingly, the aspect ratio L/h is 10. In this study, the number of rows and columns of holes is 2 and 40 for a square grid size of $30 \mu\text{m}$. The edge of square holes and the diameter of circle holes vary in the range of grid size and guarantee the fact value of fill ratio as the expression (1) ($\alpha = 0.067 \div 0.93$).

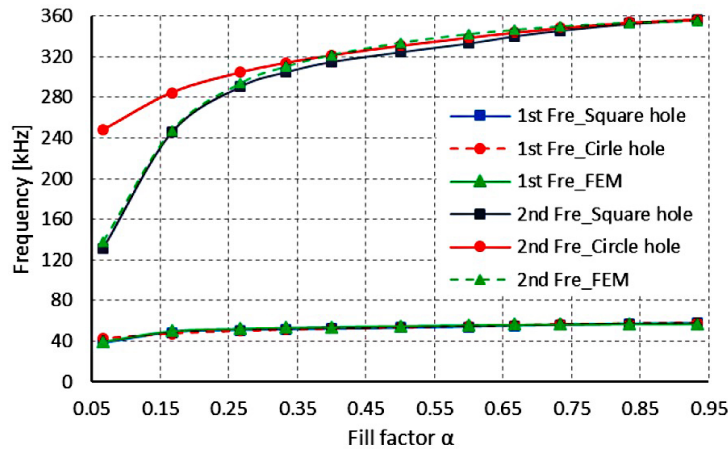


Fig. 4. The two first frequencies of the single fixed-guided perforated beam

The first two frequencies of the above single beam with cutout holes shaped with square and circle holes in two cases of boundary condition: one fixed end - one guided end (clamped-simply supported or fixed-guided beam) and 2 fixed end (clamped-clamped or fixed-fixed beam) are shown in Fig. 4 and Fig. 5, respectively. The results show that the values of the first two frequencies of a single beam increase according to the value of fill factor α , whereby the natural frequency decreases when increasing the size hole. It can be seen that the value of frequency is different according to different hole shapes. Especially, when $0.05 < \alpha < 0.4$, the variability of the frequencies increases significantly. The larger the hole size, the more obvious the difference. This variation occurs more intensely in the case of the square holes. When α varies in the interval $[0.4-1]$, the values of the natural frequencies are similar in both forms of holes, and at the same time, the frequency variation seems to be linear. The different boundary conditions produce different natural frequencies. The first two frequencies in the case of fixed-fixed beam are larger than in fixed-guided beam. The increase is 6.3 and 2.7 times for the first and the second frequency respectively. These results also show that the FEM analysis is in good agreement with the simulation analysis in the square holes.

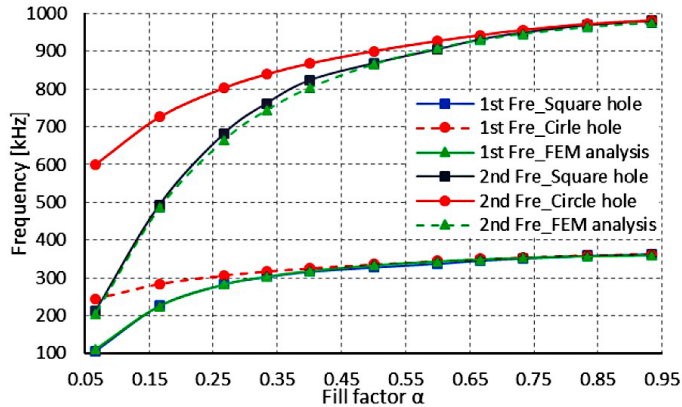


Fig. 5. The two first frequencies of the single fixed-fixed perforated beam

3.2. Mechanical response of a micro-perforated beam with crab structure

In most practical structures, the equivalent stiffness directly contributes to the resonant frequency of the resonators, including microresonators. The equivalent stiffness of the beam is an essential factor in designing a mechanical vibrational structure. The higher the stiffness, the less deflection that will occur, and the higher the operating frequency of the system. Determining this equivalent stiffness is held in simulation based on the assumption about the linear behavior of the beam material. The regular formula

expresses the relationship between deformation δ and stiffness k of the beam as:

$$k = \frac{F}{\delta}. \tag{11}$$

The crab-shaped beam is created from two perpendicular single bars creating the L-shape (or “Crab” shape in Fig. 1). The lengths of the two bars are 200 and 300 μm ; their wide and thickness are 16 and 30 μm both of them. To determine the equivalent stiffness of the beam, a unit force (1 μN) is loaded at the end of the beam in the vibration direction. The displacement obtained from the ending beam depends on the properties of the beam material, geometrical parameters, and boundary conditions of the beam. The size and the number of holes also vary the equivalent stiffness. The holes in this beam are chosen in square and circle shape. In each branch of this crab beam, the holes are distributed in one line along the length of each beam segment.

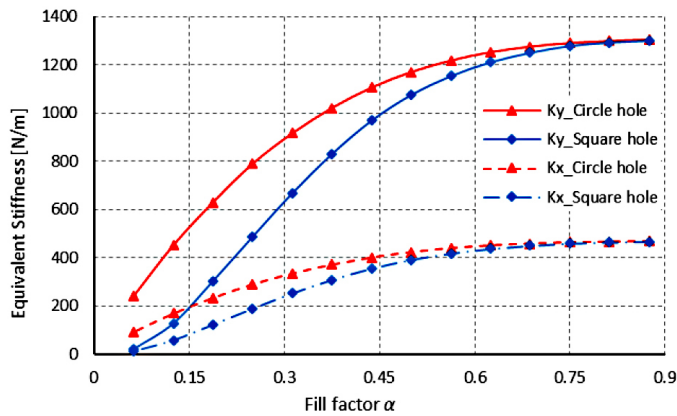


Fig. 6. The equivalent stiffness of the crab-shaped perforated beam

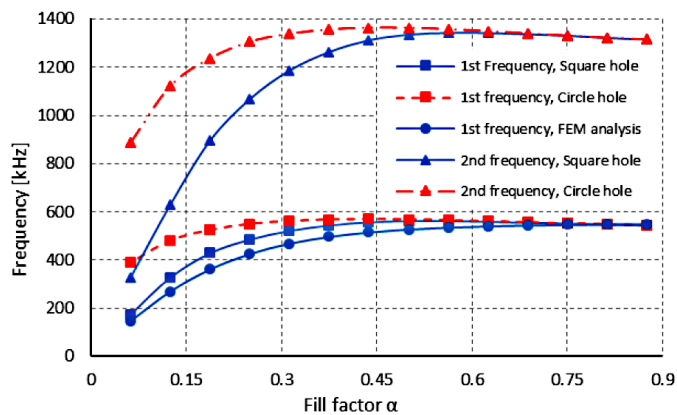


Fig. 7. Two first resonant frequencies of the crab-shaped perforated beam

Fig. 6 and Fig. 7 describe the influence of the size hole on the mechanical response of the crab-shaped beam with one line of square and circle holes in-plane of the beam. Where the equivalent stiffness in the x -direction (K_x) varies over a large range ($15 \div 460$ N/m according to $\alpha = 0.065 \div 0.875$, respectively), while the equivalent stiffness in the y -direction (K_y) varies larger ($22 \div 1300$ N/m as α above) with one fixed ending and another one guided ending of the crab beam (Fig. 6).

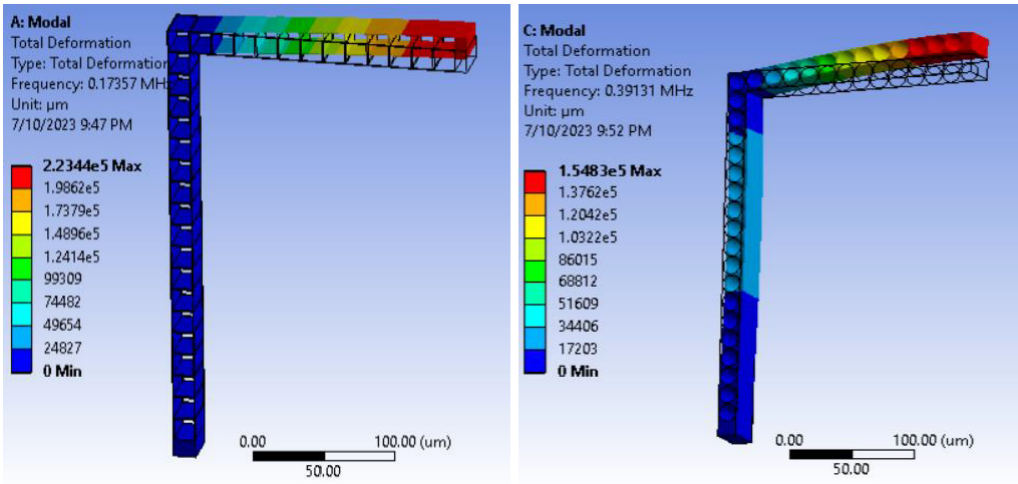


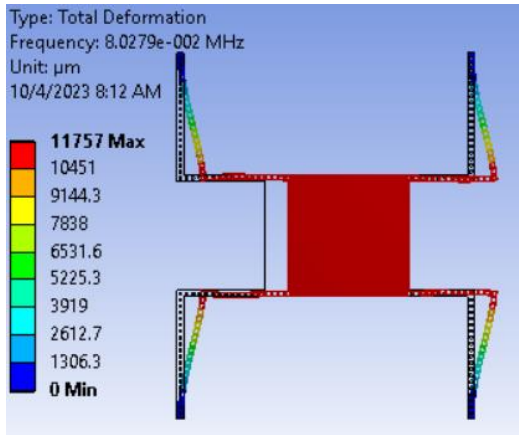
Fig. 8. The first mode shape of the beam with square holes (left) and circle holes (right)

The two first resonant frequencies consisting of the x -direction vibrational mode for the first mode and y -direction one for the second mode of this beam are shown in Fig. 7 and the configurations of the first mode in 2 types of holes are pictured in Fig. 8. The difference between two modes is narrow with small fill factor ($\alpha < 0.2$), especially in square hole. This deviation increases and remains by increasing α toward nearly 1 ($0.4 < \alpha < 0.9$). Fig. 7 also shows the fitting of analytical calculation and simulation for the first frequency in less than 10% error for the square hole. In the case of square holes, the value of both mechanical parameters is smaller than when circle holes. The results show that the mechanical response of the crab-shaped beam varies narrowly in the case of the fill factor toward nearly 1, corresponding to the size $d < 8 \mu\text{m}$. These results show that the mechanical response of the beams perforated with circle holes varies more smoothly than those with square holes.

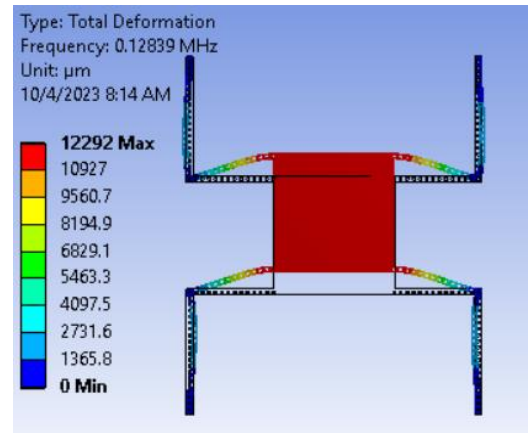
3.3. A MEMS vibratory gyroscope model with perforated crab beams

The presented MVG in this section consists of one proof mass suspended on the substrate thanks to four crab-shaped beams. These beams allow the proof mass to freely vibrate in two perpendicular directions to create two major modes called primary and

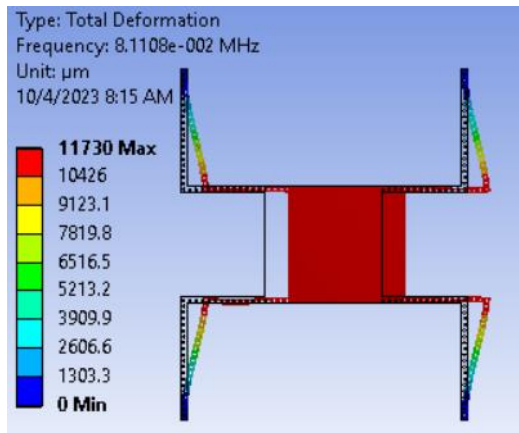
secondary modes (or driving and sensing modes) of the MVG. Each elastic beam is considered an equivalent spring, so the presented MVG becomes a 2-degree-of-freedom mechanical system with four equivalent springs connected parallelly. The 3D model and their two major modes in the case of full-fill material were introduced in [3]. In this study, the proof mass of the MVG is remained solid while four crab beams are perforated by square and circle holes sequence.



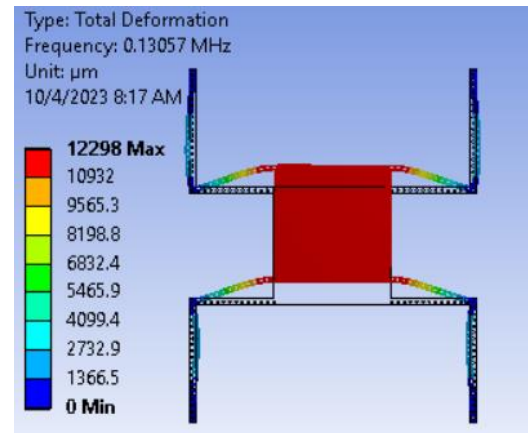
(a) Driving mode with square hole



(b) Sensing mode with square hole



(c) Driving mode with circle hole



(d) Sensing mode with circle hole

Fig. 9. Two major modes of the presented MVG

In the case of full-fill material, the values of two major frequencies are 81.525 kHz and 132.46 kHz for driving mode and sensing mode, respectively [3]. In this analysis, the driving and sensing frequency of the MVG in the case of the elastic beam perforated with the square hole and the circle hole are parameters that need to be determined. The size

of the hole is chosen as $d = 6 \mu\text{m}$, then fill factor $\alpha = 0.625$ respectively. The FEM analysis gives the obtained two major frequencies to be 80.279 kHz, 128.39 kHz (Figs. 9(a), (b)) and 81.108 kHz, 130.57 kHz (Figs. 9(c), (d)), correspondingly.

In fact, the frequencies of two desired modes (drive and sense modes) should be matched to amplify the output signal on sense mode. The frequency deviation between the two major modes needs to be considered with a suitable value to ensure the bandwidth of the MVG. In this study, the optimization for the parameter geometric is not considered. So the bandwidth in all cases is so large and does not yet suit the desired value deviation frequency.

Table 2. The two major frequencies of the presented MVG

| Presented MVG | Full fill [3] | Square hole | Error | Circle hole | Error |
|-------------------------|---------------|-------------|-------|-------------|-------|
| Driving frequency (kHz) | 81.525 | 80.279 | 1% | 81.108 | 1% |
| Sensing frequency (kHz) | 132.46 | 128.39 | 3% | 130.57 | 1% |
| Bandwidth (kHz) | 50.935 | 48.111 | 6% | 49.462 | 3% |

The results in Table 2 show that the value of the two major frequencies decreases with the presence of holes. The square holes cause a faster decrease than the circle holes. Besides, the frequency deviation also decreases thanks to the holes, and thence bandwidth can be optimized by not only changing the geometrical parameters of beams (length, width, and thickness) but also the size of the hole cut out of the beams. The error of the frequency compared with the full-fill model is less than 3%.

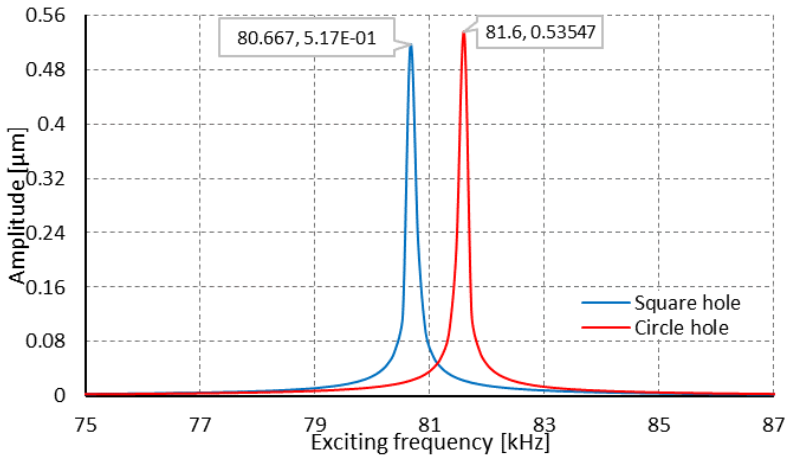


Fig. 10. The Amplitude-Frequency response of MVG with perforated crab beam

The driving frequency of the proposed MVG is reconfirmed by the harmonic response analysis in the ANSYS project. This analysis allows to determine the resonant

frequency of the system in case of the exciting force loaded in the structure for vibration in the desired direction. These frequencies are determined with maximum amplitude at 80.667 kHz and 81.6 kHz for the square hole and the circle hole respectively (error 0.4% and 0.6% comparing with the results in Table 2).

4. CONCLUSION

The paper introduced the dynamic response of the microbeam with the crab shape and cut-out hole in the body of the beam. The obtained results show that the hole size significantly reduces the equivalent stiffness of the perforated beams, then reduces the resonant frequency of the whole Crab shape beam and the whole MVG system model including four micro crab perforated beams. The driving frequency of the crab MVG model is determined in the square and circle holes as 80.667 kHz and 81.6 kHz with errors of 0.4% and 0.6% respectively. The deviation of frequency in the driving mode is less than 3% compared with the full-fill model. This research shows that the presence of the perforated holes causes a decrease in the equivalent stiffness of beams and thence decreases the operating frequencies of the system. Besides, the effect of cut-out holes on the damping force needs to be analyzed to improve the dynamic response of the whole crab MVG model in subsequent studies.

DECLARATION OF COMPETING INTEREST

The authors declare that they have no known competing financial interests or personal relationships that could have appeared to influence the work reported in this paper.

FUNDING

This research received no specific grant from any funding agency in the public, commercial, or not-for-profit sectors.

REFERENCES

- [1] D. Van Hieu, L. Van Tam, N. Van Duong, N. Duy Vy, and C. Manh Hoang. Design and simulation analysis of A Z axis microactuator with low mode cross-talk. *Journal of Mechanics*, **36**, (2020), pp. 881–888. <https://doi.org/10.1017/jmech.2020.48>.
- [2] H. Din, F. Iqbal, and B. Lee. Modelling and optimization of single drive 3-axis MEMS gyroscope. *Microsystem Technologies*, **26**, (2020), pp. 2869–2877. <https://doi.org/10.1007/s00542-020-04840-7>.
- [3] V. T. Vu and D. T. Chu. Determine the dynamic parameters in mechanical system of the crab-shaped MEMS vibratory gyroscope. *Microsystem Technologies*, **27**, (2021), pp. 3429–3435. <https://doi.org/10.1007/s00542-020-05128-6>.

- [4] S. E. Alper and T. Akin. Symmetrical and decoupled nickel microgyroscope on insulating substrate. *Sensors and Actuators A: Physical*, **115**, (2004), pp. 336–350. <https://doi.org/10.1016/j.sna.2004.04.041>.
- [5] K. T. Hoang, D. T. Nguyen, and P. H. Pham. Impact of design parameters on working stability of the electrothermal V-shaped actuator. *Microsystem Technologies*, **26**, (2019), pp. 1479–1487. <https://doi.org/10.1007/s00542-019-04682-y>.
- [6] K. Guha, H. Dutta, J. Sateesh, S. Baishya, and K. Srinivasa Rao. Design and analysis of perforated MEMS resonator. *Microsystem Technologies*, **27**, (2018), pp. 613–617. <https://doi.org/10.1007/s00542-018-4207-5>.
- [7] K. Guha, N. M. Laskar, H. J. Gogoi, K. L. Baishnab, and K. S. Rao. A new analytical model for switching time of a perforated MEMS switch. *Microsystem Technologies*, **26**, (2018), pp. 3143–3152. <https://doi.org/10.1007/s00542-018-3803-8>.
- [8] M. A. Alazwari, A. A. Abdelrahman, A. Wagih, M. A. Eltaher, and H. E. Abd-El-Mottaleb. Static analysis of cutout microstructures incorporating the microstructure and surface effects. *Steel and Composite Structures*, **38**, (5), (2021), pp. 583–597. <https://doi.org/10.12989/scs.2021.38.5.583>.
- [9] K. Guha, N. M. Laskar, H. J. Gogoi, S. Chanda, K. L. Baishnab, K. S. Rao, and N. P. Maity. An improved analytical model for static pull-in voltage of a flexured MEMS switch. *Microsystem Technologies*, **26**, (2018), pp. 3213–3227. <https://doi.org/10.1007/s00542-018-3911-5>.
- [10] L. Luschi and F. Pieri. An analytical model for the determination of resonance frequencies of perforated beams. *Journal of Micromechanics and Microengineering*, **24**, (2014). <https://doi.org/10.1088/0960-1317/24/5/055004>.
- [11] T. Ozaki, N. Ohta, and M. Fujiyoshi. Analytical modeling of a MEMS beam resonator with release-etch holes. *Journal of Micromechanics and Microengineering*, **32**, (2022). <https://doi.org/10.1088/1361-6439/ac809a>.
- [12] S. M. Han, H. Benaroya, and T. Wei. Dynamics of transversely vibrating beams using four engineering theories. *Journal of Sound and Vibration*, **225**, (1999), pp. 935–988. <https://doi.org/10.1006/jsvi.1999.2257>.
- [13] Y. Song, T. Kim, and U. Lee. Vibration of a beam subjected to a moving force: Frequency-domain spectral element modeling and analysis. *International Journal of Mechanical Sciences*, **113**, (2016), pp. 162–174. <https://doi.org/10.1016/j.ijmecsci.2016.04.020>.
- [14] A. A. Abdelrahman, M. A. Eltaher, A. M. Kabeel, A. M. Abdraboh, and A. A. Hendi. Free and forced analysis of perforated beams. *Steel and Composite Structures*, **31**, (5), (2019). <https://doi.org/10.12989/scs.2019.31.5.489>.